Energy dissipation measures in three-dimensional disordered porous media

H. Başağaoğlu*
Idaho National Laboratory, P.O. Box 1625, MS 2025, Idaho Falls, Idaho 83415, USA

P. Meakin
Idaho National Laboratory, P.O. Box 1625, MS 2211, Idaho Falls, Idaho 83415, USA

S. Succi
Istituto Applicazioni Calcolo, CNR-IAC Viale del Policlinico 137, 00161, Rome, Italy
(Received 16 May 2005; published 4 October 2005)

The onset of nonlinear flow was analyzed in three-dimensional random, porous granular systems with 60% porosity using a lattice-Boltzmann model. Quantitative analysis was based on participation numbers built on local kinetic energies and energy dissipation rates computed via nonequilibrium kinetic (viscous stress) tensors. In contrast to the kinetic energy participation number, which characterizes the onset of nonlinearity in terms of a transition from a locally concentrated to a dispersed distribution of kinetic energy densities, the nonequilibrium kinetic tensor participation number characterizes the onset of nonlinearity in terms of a transition from a dispersed to a locally concentrated distribution of energy dissipation densities as the flow rate increases. The transition characterized by the nonequilibrium kinetic tensor participation number occurred over a nearly equal or a narrower range of Reynolds numbers when compared to the transition characterized by the kinetic energy participation number.

DOI: 10.1103/PhysRevE.72.046705 PACS number(s): 47.11.+j, 47.55.Mh

In a wide range of natural and experimental systems, the single-phase flow of fluids through porous media can be accurately described by the Darcy relationship between the average fluid flow velocity $\mathbf{u}$ and the hydraulic potential gradient, $(\nabla P - \rho \mathbf{g})$, where P is the fluid pressure, ρ is the fluid density, and $\mathbf{g}$ is the gravitational acceleration. The Darcy equation has been used extensively to simulate groundwater flow [1] and fluid flow in oil reservoirs during oil recovery [2]. In these applications, the fluid velocities are small and the Darcy equation provides accurate predictions throughout most of the flow domain. However, in the vicinity of high-rate production and injection wells, the Darcy equation may become inaccurate [3].

The Darcy relationship is accurate only if the ratio between inertial forces and viscous forces (the Reynolds number) is sufficiently small. In a heterogeneous porous medium, the flow is concentrated onto preferred pathways, which pass through high permeability regions determined by the spatial distribution of permeability associated with the pore morphology. Because of the nonuniform spatial distribution of fluid flow velocities, the deviations from linear flow behavior are also nonuniform, and nonlinear effects appear in some regions before others, if the mean flow velocity is increased monotonically from a small value. The Forchheimer equation,

$$-(\nabla P - \rho \mathbf{g}) = \frac{\mu}{k}\mathbf{u} + \beta \mathbf{u}|\mathbf{u}|, \tag{1}$$

where μ is the dynamic viscosity of the fluid, β is the non-Darcy flow coefficient, and k is the permeability of the porous medium, has been proposed (among other equations) to represent non-Darcy effects in high-velocity flow through granular porous media [3–7]. In Eq. (1), the first term on the right-hand side represents the contribution of viscous forces to the hydraulic potential gradient and the second term represents the effects of inertial forces. At low velocities, Eq. (1) reduces to Darcy's law. At high velocities in a homogeneous porous medium and in high-velocity zones in a heterogeneous porous medium, inertial effects compete with viscous effects, and deviations from Darcy's law can be expected. Based on numerical simulation results, the Forschheimer equation was reported to better characterize deviations from the Darcy equation due to inertial effects in homogeneous three-dimensional (3D) porous media than in homogeneous two-dimensional (2D) porous media [8]. Microscopic inertial, viscous, and drag forces have been studied to evaluate the mechanisms leading to nonlinear macroscopic effects in high flow velocity zones in heterogeneous porous media. Through an order of magnitude analysis, increased microscopic viscous forces ($\mu \nabla^2 \mathbf{u}$) at pore walls (drag forces) were reported to be the leading mechanism responsible for the onset of nonlinearity [9], but the authors also proposed that both microscopic inertial ($\rho \mathbf{u} \cdot \nabla \mathbf{u}$) and viscous effects could be important, particularly for high Reynolds number flows through coarse-grained porous media. For a homogeneous and ordered flow domain with periodic boundaries, the nonlinearity was attributed to pressure and viscous drag forces at the solid-fluid interfaces [8]. In other studies, the nonlinearity was related to microscopic inertial forces [6,10,11]. These results revealed that local characteristics of the pore geometry (size, shape, and connectivity) determine the balance between microscale viscous, inertial, and drag forces. Hence, the relative magnitudes of the momentum transfer mechanisms could vary from one region to another

*Present address: Department of Geosciences, Oregon State University, Corvallis, Oregon 97331, USA.

in the tortuous flow domain in heterogeneous and disordered porous systems.

The mean values of the microscopic forces computed at different Reynolds numbers ($\mathrm{Re}=|u|l/\nu$, where $|u|$ is the average velocity of the fluid in the pore throat, l is the throat diameter, and ν is the kinematic viscosity) have been used to study nonlinear effects in high-velocity flow regimes [5]. An alternative approach is to determine participation numbers, which characterize the uniformity of the flow through the porous medium. The transition of an incompressible, single-phase, athermal, Newtonian fluid from linear to nonlinear flow through a high-porosity (90%) 2D disordered porous media was quantified through a participation number based on the distribution of the local kinetic energy density [6], π,

$$\pi \equiv \left(n \sum_{i=1}^{n} q_i^2 \right)^{-1}, \tag{2}$$

where n is the total number of grid nodes. q_i accounts for the contribution of the local kinetic energy at lattice node i to the total kinetic energy of the system, and it is given by $q_i = \phi_i / \Sigma_{j=1}^{n} \phi_j$, where $\phi_i = u_{xi}^2 + u_{yi}^2 + u_{zi}^2$, and u_{xi}, u_{yi}, and u_{zi} are the Cartesian components of the flow velocity $\mathbf{u}$. For uniform flow, $q_i \cong 1/n$ for all i, and $\pi \cong 1$. In the limit in which the flow is concentrated onto a single node q would have a value of unity for that node and zero for the other nodes, so that π would have a value of $1/n$. In general, $1/n \leqslant \pi \leqslant 1$, and π characterizes the nonuniformity of the flow. The local kinetic energy based participation number captures the effects of inertial forces near the onset of nonlinearity in flows across 2D systems [6]. Although, the local kinetic energy was used as a statistical indicator, the pressure field and viscous stress also varied spatially. Hence, alternative participation numbers, based on these observables can be constructed to characterize the onset of nonlinear effects. In homogeneous and ordered porous media, the contribution of drag forces at solid-fluid interfaces relative to the contribution of viscous forces was found to be larger for 3D systems than for 2D systems with the same porosity [8].

The main objective of this article is to explore statistical indicators of deviations from Darcian flow in 3D disordered porous media. Participation numbers based on momentum energy dissipation rates computed through nonequilibrium kinetic tensors were used in this work in addition to previously proposed participation numbers based on local kinetic energy densities to analyze the onset of nonlinear effects as the flow rate is increased. A 3D lattice-Boltzmann (LB) model was used to simulate gravity-driven flow in synthetic porous media. LB models are based on local particle velocity distributions that define the populations of fluid particles moving from each node of a regular lattice toward a discrete set of neighboring nodes [12]. The discretized Lattice-Boltzmann equation with a single relaxation time (Bhatnagar-Gross-Krook) model [13] can be written as

$$f_k(\mathbf{x} + \mathbf{e}_k \Delta t, t + \Delta t) - f_k(\mathbf{x}, t) = \frac{[f_k^{eq}(\mathbf{x}, t) - f_k(\mathbf{x}, t)]}{\tau}, \tag{3}$$

where f_k is the population density along the velocity vector $\mathbf{e}_k$, f_k^{eq} is the equilibrium Maxwell-Boltzmann distribution function, τ is the relaxation parameter, $\mathbf{x}$ is the position of a lattice node, and Δt is the time increment. A 3D 19-velocity (D3Q19) model was used in this study. The discrete velocity vector basis for the D3Q19 model consists of the null vector, six vectors of length unity directed toward the nearest neighbor nodes, and twelve vectors of length $\sqrt{2}$ directed toward the next-nearest neighbor nodes. The equilibrium Maxwell-Boltzmann distribution is approximated by the low-Mach number mass and momentum conserving expansion [14]

$$f_k^{eq} = w_k \rho \left(1 + \frac{e_{k\alpha} u_\alpha}{c_s^2} + \frac{Q_{k\alpha\beta} u_\alpha u_\beta}{2 c_s^4} \right), \tag{4}$$

where w_k is the weight coefficient for the kth vector (1/3 for the null vector, 1/18 for the nearest neighbor vectors, and 1/36 for the next-nearest neighbor vectors). $Q_{k\alpha\beta} = e_{k\alpha} e_{k\beta} - c_s^2 \delta_{\alpha\beta}$ is the projector along the kth direction, where $\delta_{\alpha\beta}$ is the Kronecker delta that takes a value of 1 when $\alpha = \beta$, and 0 otherwise $(\alpha, \beta = \{x, y, z\})$. The local macroscopic density and velocity at a lattice site can be computed from the distribution functions at that site as $\rho = \Sigma_{k=0}^{18} f_k$ and $\rho \mathbf{u} = \Sigma_{k=0}^{18} f_k \mathbf{e}_k$. With the equilibrium distribution in Eq. (4), the Navier-Stokes equations can be recovered through the Chapman-Enskog expansion, which shows that the kinematic viscosity of the fluid is $\nu = c_s^2(\tau - 1/2)$, and the sound velocity is $c_s = 1/\sqrt{3}$. In the low-Mach number limit, the LB model simulates nearly incompressible fluid dynamics. A second order-accurate half-way bounce-back scheme [12,15] was used to simulate no-slip boundary condition at the surfaces of the spherical grains in the granular porous media. Periodic boundary conditions were imposed at the surface of the computational domain. Participation numbers based on the momentum flux tensor are proposed as an alternative to participation numbers based on the local kinetic energy. The population distribution function f can be split into local equilibrium and nonequilibrium components, $f = f^{eq} + f^{neq}$, with the assumption that $f^{neq} \approx O(\epsilon) f^{eq}$, where ϵ is the Knudsen number. The equilibrium part of the velocity distribution is associated with the nondissipative component of the momentum flux tensor Ψ^{eq}, and the nonequilibrium part of the velocity distribution is associated with the viscous (dissipative) component of the momentum flux tensor Ψ^{neq} [12,15,16],

$$\Psi_{\alpha\beta}^{eq} \equiv \int m u_\alpha u_\beta f^{eq} d\mathbf{u}, \quad \Psi_{\alpha\beta}^{neq} \equiv \int m u_\alpha u_\beta f^{neq} d\mathbf{u}. \tag{5}$$

From the momentum conservation equations, $\nabla \cdot \Psi^{eq} \equiv \mathbf{u} \cdot \nabla \mathbf{u} + \nabla P$ and $\nabla \cdot \Psi^{neq} \equiv \nabla \cdot \boldsymbol{\tau}$, where $\boldsymbol{\tau}$ is the shear stress tensor. Fluctuations in the flow field are damped by the viscous dissipation, particularly when the inertial forces are smaller than or comparable to viscous forces (at low Re). The kinetic nonequilibrium tensor $S_{\alpha\beta}$ can be expressed in terms of f^{neq} [Eq. (6)] or local gradients of macroscopic velocities [Eq. (7)],

$$S_{\alpha\beta} \equiv \frac{1}{2 c_s^2 \tau} \sum_k f_k^{neq} Q_{k\alpha\beta}, \tag{6}$$

$$S_{\alpha\beta} \equiv \nu \varsigma_{\alpha\beta} = \frac{\nu}{2}(\partial_\alpha u_\beta + \partial_\beta u_\alpha), \tag{7}$$

where $\varsigma_{\alpha\beta}$ is the symmetric strain tensor. In the above equations, the effects of local variations in the morphology of the granular porous media on the flow regime are captured through the spatial distribution of the energy dissipation density field determined via the nonequlibrium population distributions and local velocity gradients. These two definitions of the nonequilibrium kinetic tensors must converge in the limit of small ϵ (i.e., small variations of the velocity field on the scale of the molecular mean-free path). An upwind scheme [17] was employed to approximate the velocity gradients in Eq. (7). Once the momentum flux density tensor had been computed using these two approaches, the Frobenius norm of the momentum flux, $\|S\| = (\Sigma_\alpha \Sigma_\beta S_{\alpha\beta}^2)^{1/2}$, was calculated at each lattice node. The norm of the momentum flux tensor at a lattice node is a measure of the local energy dissipation, and the corresponding participation number π_n can be computed directly from Eq. (1) by replacing ϕ_i with $\|S\|_i$.

The kinetic energy and nonequilibrium kinetic tensor participation numbers can be measured if the magnitude and the direction of pore-scale velocities can be mapped experimentally. Microparticle image velocimetry (MICROPIV) with refractive index matching has been recently developed [18] to experimentally determine pore-scale velocities in quasi-2D porous systems with equal-size pore bodies. In the context of future work, the authors discussed the potential uses of MICROPIV to measure local pore velocities for single-phase flows in more complex and realistic 3D pore geometries. Once this has been accomplished, the participation numbers discussed herein could be measured experimentally.

The model porous media were generated by randomly inserting spheres with radii r, randomly selected from a truncated Gaussian distribution (r had a mean of 12.0, a width of 6.0, and it was truncated to the range $6 \leqslant r \leqslant 24$) into a rectangular domain of size $128 \times 128 \times 128$ (all in lattice units) with periodic boundary conditions. The centers of the spheres were given random integer coordinates, and the spheres were allowed to overlap. The addition process was continued until the volume fraction of the domain occupied by the spheres reached or exceeded a target value of $\theta_T = 0.6$.

The 3D LB simulations were performed on four different realizations of the 60% porosity pore space model, representing unconsolidated porous domains. All simulations were continued up to 3000 time steps, which was sufficient to ensure that deviations from the steady-state flow regime were negligible ($<0.1\%$). The spatial distribution of the solid grains and cross sections at the center of the flow domain with 60% porosity, used in the first realization, is shown in Fig. 1. Fluid flow was driven by a uniform gravitational field, and the Reynolds number was tuned by changing the gravitational acceleration, **g** acting in the **x** direction only (Fig. 1). The Reynolds number, defined in terms of geometric mean of the grain diameters, was varied over the range 0.04–16.7, which was broad enough to investigate the flow transitions.

The participation number based on local kinetic energies

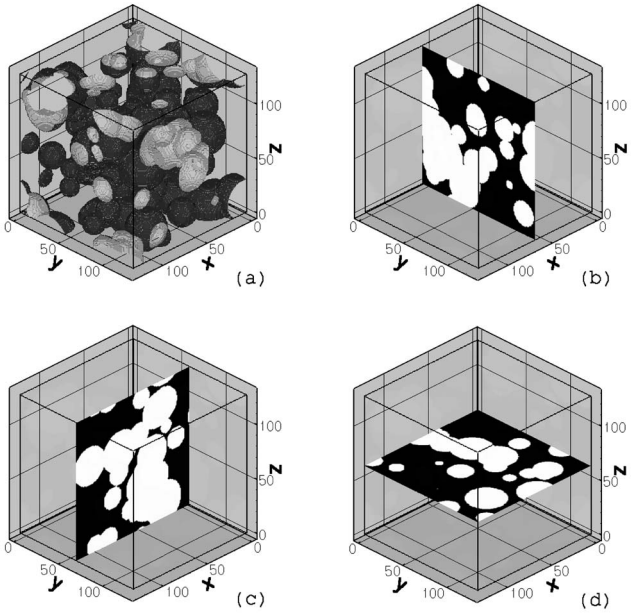

FIG. 1. A disordered 3D flow domain (a) with cross sections at the center along x, y, and z coordinates (b)–(d). White regions are occupied by soil grains and black regions are the flow zones in (b)–(d).

π increased with Re (Fig. 2), in agreement with the findings reported in Ref. [6]. As Re increased, the flow became less localized (more uniform) with increasing contributions from a larger number of grid nodes to the total global kinetic energy. Although the kinetic energy participation numbers for realizations 1 and 2 provided a relatively narrower transition from linear to nonlinear flow, the transitions for realizations 3 and 4 were broader, and the critical Reynolds numbers, at which a transition to nonlinear flow occurred, displayed a wider range. On the other hand, Fig. 3 reveals that the energy dissipation (resulting from local spatial variations in macroscopic velocities) became less uniform at the onset of nonlinear effects. The spatial distribution of kinetic energy and energy dissipation measures exhibited (Fig. 4) geometric anisotropy (i.e., directional dependency of the correlations), with positive correlations in the y (relatively strong) and z

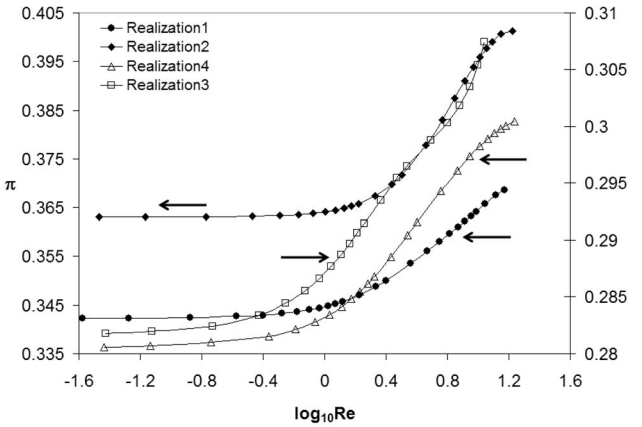

FIG. 2. Participation numbers based on local kinetic energies. Right axis is reserved for realization 3.

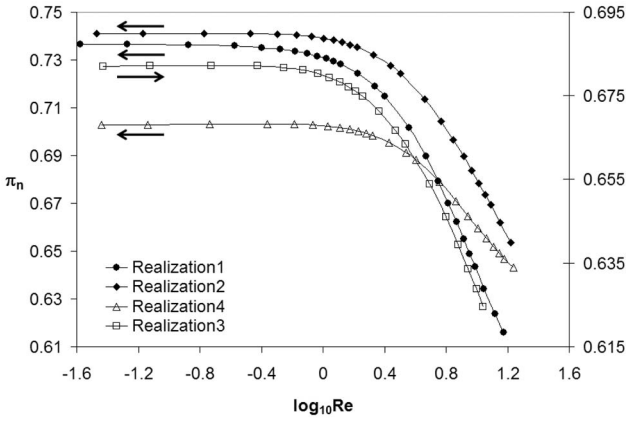

FIG. 3. Participation numbers based on nonequilibrium kinetic tensors. Right axis is reserved for realization 3.

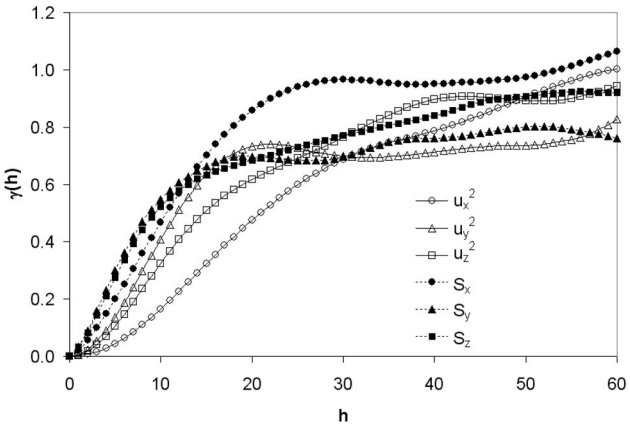

FIG. 4. Semivariograms γ in different spatial coordinates for realization 4 (similar behavior was also observed for the other realizations). $\gamma(\mathbf{h})=C(\mathbf{0})-C(\mathbf{h})$ [20], in which $\mathbf{h}$ is the distance vector and C is the covariance. $\gamma(\mathbf{h})=0$ represents the perfect correlation, and $\gamma(\mathbf{h})=1$ indicates no correlation.

(relatively weak) directions, perpendicular to the direction of the gravitational filed. The spatial variance was computed through the spatial covariance, $C(\mathbf{h})\equiv\Sigma_{\mathbf{h}}Y(\mathbf{x}+\mathbf{h})Y(\mathbf{x})/(n-1)$. Here, $Y(\mathbf{x})$ is the standard normal form of the energy or energy dissipation measure obtained by subtracting the sample mean from each measure and dividing by the sample standard deviation, and n is the number of data points. The variogram analyses consistently revealed shorter scale spatial correlations (more localized behavior) for the energy dissipation measures than the energy measures, particularly in the direction of $\mathbf{g}$, for all realizations. Although these measures convey different information on the flow characteristics (local velocities vs spatial variations in local velocities), both characterize the onset of nonlinear effects as the Reynolds number increases. When compared to flow transitions characterized by the kinetic energy participation number, the nonequilibrium kinetic tensor participation number resulted in nearly equal or narrower flow transitions for all realizations (Fig. 3). π_n's based on Eq. (6) and Eq. (7) produced similar trends for all realizations with up to 1–1.5% differences at low flow rates and 3–4% differences at high flow rates.

To calculate the critical Reynolds number, the participation number curves were fitted by cubic splines [17] and an increase of 0.5% with respect to the first sampling point was used as an indicator of the onset of the flow transition. The critical Reynolds numbers obtained from the kinetic energy participation number π were 1.31, 1.79, 0.96, and 0.80, while the critical Reynolds numbers obtained from the energy dissipation participation numbers π_n were 1.03, 1.79, 1.67, and 1.72. The energy dissipation participation numbers π_n provided nearly equal or narrower transitions for the four flow fields and yielded 72–116% higher critical Reynolds numbers for the third and fourth realizations than the kinetic energy participation numbers. In summary, the present 3D analysis shows that different statistical indicators provide complementary characterization of flow transitions in porous media. We propose that participation numbers based on energy dissipation [19], i.e., nonequilibrium kinetic tensor, provide a useful indicator (in addition to the kinetic energy participation number) for the quantitative assessment of flow transitions in heterogeneous porous media (Fig. 2 and Fig. 3).

ACKNOWLEDGMENT

This work was supported by the U.S. Department of Energy Environmental Management Science Program under Contract No. DE-AC07-05ID14517 at the Idaho National Laboratory.

[1] M. A. Robinson and W. G. Reay, Ground Water **40**, 123 (2002).
[2] T. Ahmed, *Reservoir Engineering Handbook* (Elsevier, London, 2001).
[3] J. Bear, Dynamics of Fluids in Porous Media (American Elsevier, New York, 1972).
[4] E. V. Evans and R. D. Evans, JPT, J. Pet. Technol. **40**, 1343 (1988).
[5] H. Ma and D. W. Ruth, Transp. Porous Media **13**, 139 (1993).
[6] J. S. Andrade, Jr., U. M. S. Costa, M. P. Almeida, H. A. Makse, and H. E. Stanley, Phys. Rev. Lett. **82**, 5249 (1999).
[7] Y.-S. Wu, Transp. Porous Media **49**, 209 (2002).
[8] M. Fourar, G. Radilla, R. Lenormand, and C. Moyne, Adv. Water Resour. **27**, 669 (2004).
[9] S. J. Hassanizadeh and W. G. Gray, Transp. Porous Media **2**, 521 (1987).
[10] A. Z. Barak, Transp. Porous Media **2**, 533 (1987).
[11] V. D. Cvetkovic, Transp. Porous Media **1**, 63 (1986).
[12] S. Succi, *The Lattice-Bolzmann Equation* (Oxford University Press, New York, 2001).
[13] P. L. Bhatnagar, E. P. Gross, and M. A. Krook, Phys. Rev. **94**, 511 (1954).

[14] Y. H. Qian, D. D'Humieres, and P. Lallemand, Europhys. Lett. **17**, 479 (1992).
[15] A. J. C. Ladd, J. Fluid Mech. **271**, 285 (1994).
[16] R. Benzi, S. Succi, and M. Vergassola, Phys. Rep. **222**, 145 (1992).
[17] J. H. Ferziger, *Numerical Methods for Engineering Applications* (Wiley-Interscience, New York, 1998).
[18] B. Zerai, B. Z. Saylor, J. R. Kadambi, M. J. Oliver, A. R. Mazaheri, G. Ahmadi, G. S. Bromhal, and D. H. Smith, Transp. Porous Media **60**, 159 (2005).
[19] M. Pilotti, S. Succi, and G. Menduni, Europhys. Lett. **60**, 72 (2002).
[20] E. Gringarten and C. V. Deutsch, Math. Geol. **33**, 507 (2001).